BAMS Article

Anomalous Propagation and the Sinking of the Russian Warship *Moskva*

Lars Norin, Niklas Wellander, and Abhay Devasthale

KEYWORDS: Atmosphere; Radars/Radar observations; Reanalysis data; Sea/ocean surface; Inversions

ABSTRACT: On 13 April 2022, the Russian warship *Moskva* was hit by two Ukrainian Neptune anti-ship missiles in the Black Sea, leading to its demise. Before launching an anti-ship missile, a target must first be detected and positioned, for example, by an accompanying radar system. However, when the missiles hit the *Moskva* she was well beyond the normal radar horizon of any ground-based radar system, making the ship undetectable under normal circumstances. Using meteorological reanalysis data, we show that at the time of the missile launch the prevailing weather conditions allowed a ground-based radar to detect targets far beyond the normal radar horizon through anomalous propagation conditions. During such conditions, the atmospheric index of refraction decreases rapidly with height, making electromagnetic radiation bend downward to, partly or fully, compensate the curvature of the Earth. The results show that atmospheric conditions must be considered carefully, even during warfare, as their impact on radar wave propagation can be considerable.

SIGNIFICANCE STATEMENT: Electromagnetic waves, such as those emitted by radars, are refracted by the atmosphere. Occasionally, atmospheric conditions can cause large changes in radar detection distances. In this work, we examine how a ground-based Ukrainian radar system detected the Russian warship *Moskva*, even though the ship was located far beyond the normal radar horizon. Once detected, the warship was targeted by anti-ship missiles and sunk. To characterize the atmosphere we used meteorological reanalysis data and, together with a wave propagation model, we found that the radar would have been able to detect the warship at the time of the missile launch. Other military or civilian events can likely also be clarified and better understood when supported by reanalyzed meteorological data.

https://doi.org/10.1175/BAMS-D-23-0113.1
Corresponding author: Lars Norin, lars.norin@foi.se
In final form 19 October 2023

AFFILIATIONS: Norin—Department of Radar Electronic Warfare Systems, Swedish Defence Research Agency, Linköping, Sweden; **Wellander**—Department of Radar Systems, Swedish Defence Research Agency, Linköping, and Department of Mathematical Sciences, Luleå University of Technology, Luleå, Sweden; **Devasthale**—Meteorological Research Unit, Swedish Meteorological and Hydrological Institute, Norrköping, Sweden

On 14 April 2022, news media around the world reported that explosions had occurred the previous day on the Russian warship *Moskva* in the Black Sea (Forgey and Ward 2022; Harding et al. 2022). A few days later, it was reported that the *Moskva* had sunk as a result of the damage she sustained (Hallam et al. 2022). It later became clear that the explosions were the result of the warship being hit by two Ukrainian R-360 Neptune anti-ship missiles (Ukrinform 2022).

The Ukrainian R-360 Neptune anti-ship missile system has an accompanying search-and-track radar, Mineral-U, which detects surface targets and provides the targets' coordinates to the missile launcher (Defense Express 2021b). Given that the *Moskva* at the time of the missile launch was located far beyond the normal radar horizon of any ground-based radar system (Sutton 2022), it has been an open question of how the Mineral-U radar was able to detect the warship on 13 April 2022. Since a target must be detected before launching the missiles, some have speculated that *Moskva*'s coordinates were provided by U.S. aircraft (Volkmann and Grylls 2022), but this has been denied (Cooper et al. 2022).

In December 2022, an article published in the newspaper *Ukrainska Pravda* pointed to a different explanation: the weather conditions on 13 April 2022 enabled the Mineral-U radar to extend its range to detect the *Moskva* (Romaniuk 2022). The news article bases its claim on multiple interviews with military personnel that were involved in the firing of the missiles. According to the *Ukrainska Pravda*, the crew operating the R-360 Neptune anti-ship missile system detected a large target on their radar at approximately 1600 local time [local time (LT) is UTC + 3 h] and, concluding that this was likely the Russian warship *Moskva*, fired two missiles within minutes.

The impact of the atmosphere on radar waves has been studied extensively for almost a century (Kerr 1951; Bean and Dutton 1966; Battan 1973). In addition to being attenuated by precipitation, radar waves are also usually refracted slightly toward the Earth due to the atmosphere's vertical inhomogeneity. A widely used model to calculate the propagation of electromagnetic waves is the effective Earth radius model, which uses a 4/3 Earth radius (Patterson 2008). Using this model, the radar horizon for "normal" atmospheric conditions can be calculated, which extends approximately 15% further than the geometric horizon (Skolnik 2001). However, the atmosphere is not always well described by this model and radar waves can be refracted more or less, depending on the prevalent meteorological conditions. During so-called anomalous propagation conditions, radar waves are refracted further downward by the atmosphere and can reach targets near the Earth's surface at distances far beyond the normal radar horizon (Turton et al. 1988).

Anomalous propagation conditions over various ocean waters have been studied experimentally in several measurement campaigns (Anderson et al. 2004; Kulessa et al. 2017; Q. Wang et al. 2018). With the advance of numerical weather prediction (NWP) models, anomalous propagation has also been examined using meteorological reanalysis data (von Engeln and Teixeira 2004; Lopez 2009). Over time, NWP models have steadily achieved

higher spatial and temporal resolution, making forecast datasets attractive candidates for studying anomalous propagation conditions (Haack et al. 2010; Ulate et al. 2019; Pastore et al. 2021).

To investigate the atmospheric conditions at the reported time and location of the Ukrainian anti-ship missile launch, we have used meteorological reanalysis data from the European Centre for Medium-Range Weather Forecasts (ECMWF). By calculating vertical profiles of the atmospheric refractivity and thereafter applying an electromagnetic wave propagation model, we have examined the claim that a ground-based radar could have detected the *Moskva* at the time of the missile launch.

Background

Large-scale meteorological conditions. Information on large-scale meteorological conditions can be obtained by studying satellite imagery. Figure 1 shows images from the

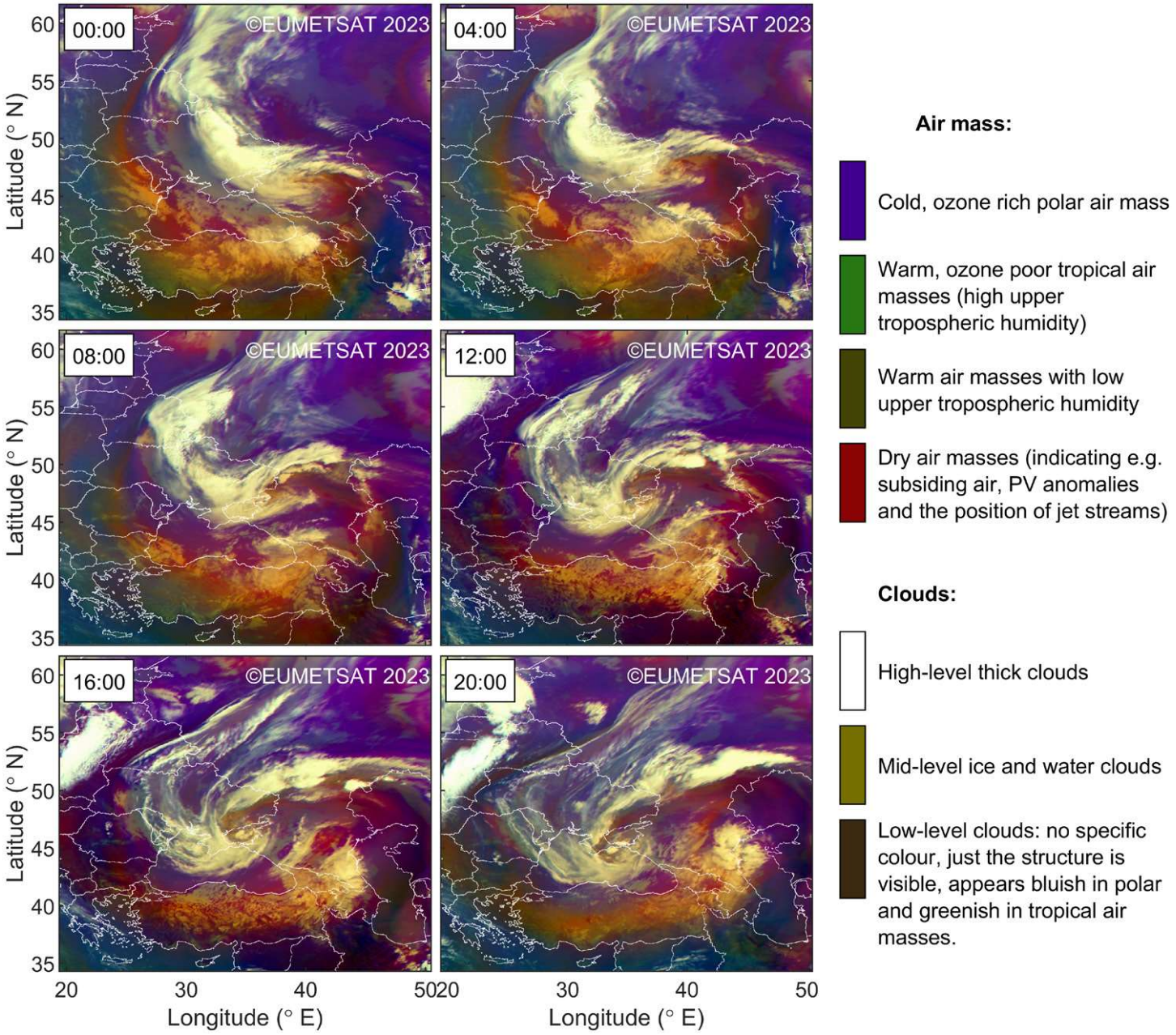

Fig. 1. Large-scale meteorological conditions near the Black Sea on 13 Apr 2022. The figures show MSG/SEVIRI images of airmass during different hours of the day. Local time (UTC + 3 h) is shown in the figures. Images were obtained from EUMETSAT (EUMETView 2023). The legend is adapted from EUMETSAT (EUMETSAT 2023) and border visibility has been enhanced.

Meteosat Second Generation (MSG) satellites for different hours of the day during 13 April 2022. MSG are geostationary meteorological satellites operated by the European Organisation for the Exploitation of Meteorological Satellites (EUMETSAT).

From the figure we can see that in the early hours of 13 April 2022, a low pressure system located in Russia, to the northeast of the Sea of Azov and to northwest of the Caspian Sea, started to strengthen and organize itself more coherently. During the day, this low pressure system moved westward and was positioned just north of the Sea of Azov in Ukraine in the late afternoon and evening hours. This resulted in the northerly cyclonic winds being aligned almost perpendicular to the Ukrainian coast and along the potential line of sight between the locations of the Mineral-U radar and the warship *Moskva*. These winds sustained for several hours from the early afternoon to the late evening on 13 April 2022, thus bringing warm and dry continental air masses over the moist and saturated lowermost marine boundary layer over the Black Sea. The capping temperature inversion locked in the moisture in the lowermost boundary layer, resulting in near-isothermal conditions. This capping temperature inversion led to strong density gradients of moisture above it, with low-level clouds moving westward while also being aligned along the line of sight between the radar and the warship.

The Mineral-U radar. The Mineral-U radar was designed to provide coordinates of surface targets to the R-360 Neptune anti-ship missile system. Once near the position of the intended target, modern anti-ship missiles like the R-360 Neptune often use onboard active radar systems to guide the missiles the final distance to the target (Genova 2018).

The Mineral-U radar entered into service of the Ukrainian army in early 2022, and its system specifications are not publicly known. However, some of its parameters can still be estimated using open sources or by using parameter values common for other, known radar systems.

The ground-based Mineral-U radar was developed from the Russian shipborne Mineral-ME radar (Defense Express 2021a). Data sheets from Mineral-ME state that its operating frequency is in the X band (8–12 GHz) (Ukrainian Defence Industry 2020b,a). In this work, we have therefore set the frequency of the Mineral-U radar to 10 GHz (i.e., $\lambda = 3$ cm).

For a radar using a reflector antenna, the radar's beamwidth can be estimated using the expression (Doviak and Zrnić 2006)

$$\theta = \frac{70\lambda}{d}, \tag{1}$$

where λ is the wavelength in meters and d is the antenna diameter in meters. Judging from photos of Mineral-U's antenna dish, its height is around 1 m (Defense Express 2021a). Using $\lambda = 3$ cm and $d = 1$ m we obtain a vertical beamwidth of $\theta \approx 2°$.

Using the size of the antenna aperture, the antenna gain G can be calculated using the expression (Skolnik 2001)

$$G = \frac{4\pi\eta A}{\lambda^2}, \tag{2}$$

where A is the size of the antenna aperture and η is the antenna efficiency. With $A = 2$ m^2 (Defense Express 2021a), $\eta = 0.6$, and $\lambda = 3$ cm we obtain $G \approx 42$ dBi. Other radar parameters are based on values from similar radars together with the authors' best guesses. The parameters we have used in our calculations are listed in Table 1.

The anti-ship missiles were reportedly launched from a position on the coastline east of Odesa (Grey zone 2022). The coastline east of Odesa has an elevation of around 20–60 m above sea level (based on the digital elevation model GTOPO30; Gesch et al. 1999). We assume

here that the Mineral-U radar was located at 46.6°N, 31.0°E (see Fig. 2) together with the missile battery and that the altitude of the radar antenna (including the mast) was 45 m above sea level. The distance at which a radar at that altitude can detect a target 20 m above sea level is, using the effective Earth radius model, approximately 46 km.

Table 1. Estimated parameters for the Mineral-U radar.

Parameter	Value	Unit
Beamwidth (θ)	2	°
Elevation angle	0	°
Polarization	H	
Required signal-to-noise ratio (S)	13	dB
Radar noise factor (F_R)	9	dB
Temperature (T_0)	290	K
Receiver bandwidth (B)	1	MHz
Internal radar losses (L_R)	5	dB
Transmit power (P_T)	10	kW
Antenna gain (G)	42	dBi
Signal processing gain (G_{SP})	0	dB
Integration gain (G_I)	10	dB
Wavelength (λ)	3	cm

***The warship* Moskva.** The warship *Moskva* was a guided missile cruiser, belonging to the *Slava* class. The ship was designed and constructed during the 1970s and *Moskva* (originally named *Slava*) was commissioned into the Soviet Union navy in 1983. At the time of construction, not much effort was put into making the ship stealthy. With a length of around 186 m and a height of more than 20 m above sea level, the ship's radar cross section (RCS) is substantial. The RCS varies with aspect angle and the largest RCS is expected from the ship's broadside (Knott et al. 2004). The broadside RCS for a ship of *Moskva*'s size is estimated to range from 40 to 50 dBsm (McGillvray 1994) while the head-on RCS can be around 10 dB lower compared to broadside (Knott et al. 2004).

The exact location of the warship at the time of the missile launch is unknown. However, the *Moskva* was observed from satellite imagery at 1852 LT, at a distance near 160 km from the northern Ukrainian shore (Sutton 2022). According to the *Ukrainska Pravda*, the *Moskva* was located some 120 km from the radar when it was hit by the missiles (Romaniuk 2022). For a more conservative estimate, we assume here that at the time of the missile launch the ship was located at 45.40°N, 30.75°E, around 135 km from the northern shore (Fig. 2).

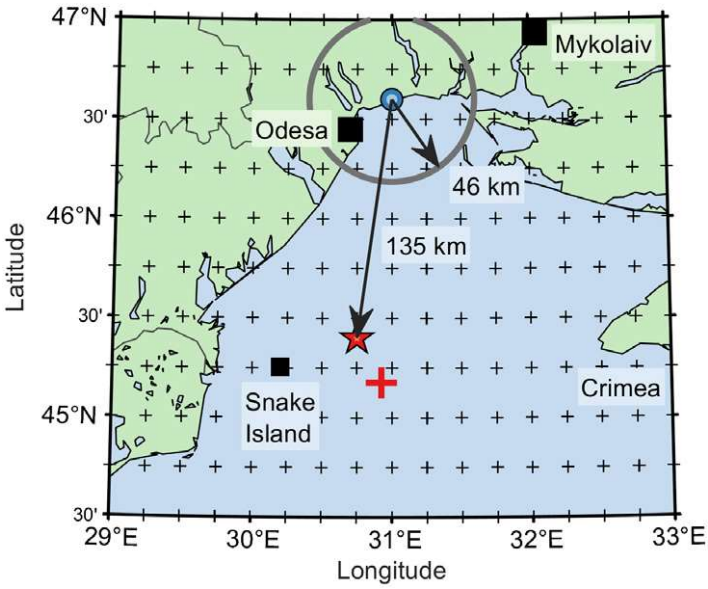

Fig. 2. Map over the Black Sea showing assumed positions of the Mineral-U radar (blue circle) and the warship *Moskva* (red star) at the time of the anti-ship missile launch. A gray circle shows the radar horizon, 46 km from the radar. A large red plus sign marks where the *Moskva* was located by satellite at 1852 LT 13 Apr 2022. Small black plus signs show grid points of the ERA5 reanalysis dataset.

Method

To investigate whether the Mineral-U radar could have detected the warship *Moskva* on 13 April 2022, we need vertical profiles of the atmospheric index of refraction, an electromagnetic wave propagation model, and a way to determine the minimum RCS of detectable targets.

Vertical profiles of the atmospheric index of refraction. Meteorological reanalysis data are based on forecasts from NWP

models. In addition to data from forecasts, reanalysis data have incorporated various meteorological observations that may not have been available at the time the forecast was made. Reanalysis data are considered to provide the most complete meteorological representation of past weather currently achievable.

In 2016, the ECMWF Reanalysis v5 (ERA5) dataset was released which provides meteorological data with 0.25° spatial resolution and hourly temporal resolution from 1940 to the present. ERA5 is produced using 4D-Var data assimilation together with ECMWF's forecast model, cycle Cy41r2. There are 137 vertical model levels in the forecast model, but the atmospheric data are interpolated to 37 pressure levels in ERA5. Data are also available on single (surface) levels. The atmospheric forecast model is coupled to a land surface model, which produces parameters such as 2-m temperature and surface pressure (Copernicus Climate Change Service 2023b).

In this work, we have used data from pressure levels, which provide global meteorological data on 37 pressure levels from 1,000 hPa up to 1 hPa (Hersbach et al. 2018a), and from single levels, providing meteorological data at or near the surface (Hersbach et al. 2018b). The ERA5 dataset is available from the ECMWF Climate Data Store (Copernicus Climate Change Service 2023c,d).

From the pressure levels dataset we have used atmospheric pressure, temperature, geopotential height, and specific humidity. The partial pressure of water vapor e was calculated using the equation (Byers 1974)

$$e = \frac{pq}{0.622 + q}, \tag{3}$$

where p is the atmospheric pressure (hPa), and q is the specific humidity (g kg^{-1}).

Geometric height H was calculated from the geopotential height z using the equation (Copernicus Climate Change Service 2023a)

$$H = R_e \frac{z}{gR_e - z}, \tag{4}$$

where R_e = 6,367.3 km is the Earth's radius at the latitude of interest and g = 9.80665 m s^{-2} is the gravitational acceleration.

For the surface level data, the available parameters are slightly different. We have used the 2-m temperature, the surface pressure, and the dewpoint temperature. Using the dewpoint temperature, the partial pressure of water vapor was calculated using the Magnus equation (Lawrence 2005)

$$e = 610.94 \exp\left(\frac{17.625 T_d}{T_d + 234.04}\right). \tag{5}$$

Here, e is the partial pressure of water vapor (Pa), and T_d is the dewpoint temperature (°C).

In the atmosphere, the index of refraction n is very close to unity. Hence, the term refractivity, $N = (n - 1) \times 10^6$, is often used. Using meteorological parameters from the reanalysis datasets, the atmospheric refractivity N can be calculated using the empirical relation (Smith and Weintraub 1953)

$$N = \frac{77.6}{T}\left(p + \frac{4810e}{T}\right), \tag{6}$$

where T is the air temperature (K), p is the atmospheric pressure (hPa), and e is the partial pressure of water vapor (hPa). For convenience, when studying anomalous propagation conditions, the modified refractivity M, which takes into account the curvature of the Earth, is often used. The modified refractivity is defined by (Turton et al. 1988)

$$M = N + \frac{H}{R_e} \times 10^6, \tag{7}$$

where H is the height above sea level in meters.

Propagation conditions are determined by the vertical gradient of the modified refractivity, dM/dH, and are often divided into different categories (Turton et al. 1988). Standard atmospheric conditions correspond to $78\,\mathrm{km}^{-1} < dM/dH \leq 157\,\mathrm{km}^{-1}$. For smaller values, $0\,\mathrm{km}^{-1} < dM/dH \leq 78\,\mathrm{km}^{-1}$, so-called superrefractive conditions occur, which increasingly bends electromagnetic waves toward the Earth. Ducting (trapping of electromagnetic waves) occurs for $dM/dH \leq 0\,\mathrm{km}^{-1}$, when the gradient of the atmospheric refractivity fully compensates the curvature of the Earth.

To calculate the propagation of radar waves, vertical profiles of the atmospheric refractivity between the position of the radar and the position of the warship were needed. We therefore interpolated the physical parameters of the ERA5 dataset (temperature, pressure, and partial pressure of water vapor) to a fixed height vector, ranging from the surface up to 3.2 km above sea level using MATLAB's "pchip" function (a shape-preserving piecewise cubic interpolation) (MathWorks 2023).

To ensure accurate modeling by the electromagnetic wave propagation model, coordinates with a range spacing of 500 m between the radar and the warship were chosen. The fixed-height, vertical profiles of temperature, pressure, and partial pressure of water vapor were bilinearly interpolated from ERA5's grid points to the selected coordinates. From these vertical profiles, the gradient of the modified atmospheric refractivity, dM/dH, was calculated.

Electromagnetic wave propagation model. The most accurate electromagnetic wave propagation models currently available solve Maxwell's equations in a given medium, supplied with appropriate boundary conditions. However, this is not possible when applied to radar signal propagation in the atmosphere. The reason is that the propagation distances of interest are very large compared to the wavelength of the radar signal, making it impossible to solve the equations numerically. One way to resolve this is to consider a two-dimensional model, describing the magnitude of the signal amplitude. This type of model is known as the parabolic equation (PE) approximation (Dockery 1988; Levy 2000).

The Swedish Defence Research Agency has developed a wave propagation model, Detvag (Asp et al. 1997), based on the PE approximation (Holm 2007). Detvag takes radar parameters (polarization, wavelength, beamwidth, antenna altitude, and elevation angle) as well as vertical profiles of the atmospheric refractivity as input. To calculate the wave propagation in a given direction, Detvag uses a two-dimensional refractivity matrix as input, if available. Thereby any changes in the atmospheric refractivity along the analyzed distance are taken into account. The Detvag wave propagation model returns the propagation factor (Patterson 2008), which is a measure of the signal's field strength relative to that of a signal in free space, as a function of range and height.

The PE approximation solved in this work is known as the narrow angle equation,

$$\frac{\partial^2 u}{\partial z^2} + 2ik\frac{\partial u}{\partial x} + k^2(n^2 - 1) = 0, \tag{8}$$

where k is the wavenumber and $n = 1 + N \times 10^{-6}$ is the index of refraction. The equation is supplied with the boundary condition

$$\frac{\partial u(x,0)}{\partial z} = -ik\xi(x)u(x,0), \tag{9}$$

where ξ is given by

$$\xi(x)=\begin{cases}\sqrt{\epsilon(x)-1}, & \text{horizontal polarization}\\ \dfrac{\sqrt{\epsilon(x)-1}}{\epsilon(x)}, & \text{vertical polarization.}\end{cases} \tag{10}$$

Here,

$$\epsilon(x)=\epsilon_{\mathrm{Re}}(x)+\frac{i\sigma(x)}{\omega\epsilon_0} \tag{11}$$

is the complex relative permittivity of the ground/sea surface, defined by the real part ϵ_{Re} and the complex part, modeled by the electrical conductivity σ. Further, ω is the angular frequency and ϵ_0 is the permittivity in vacuum. In this work we have used $\epsilon_{\mathrm{Re}} = 80$. The surface electrical conductivity of the Black Sea was assumed to be $\sigma = 2.5$ S m^{-1} (Tyler et al. 2017).

Effects from sea surface roughness and terrain at the coastline were not taken into account. Equation (8) was solved using the Fourier split-step method (Dockery 1988; Kuttler and Dockery 1991; Dockery and Kuttler 1996).

Target detection. Using the radar equation, an expression for the minimum RCS, σ_{min}, of a target required for detection can be written as (Hannen 2014)

$$\sigma_{\mathrm{min}}=\frac{S(4\pi)^3R^4F_Rk_BT_0BL_R}{P_TG^2G_{\mathrm{SP}}G_I\lambda^2\left|F_b\right|^4} \tag{12}$$

where S is the required signal-to-noise ratio, R is the distance from the radar to the target, F_R is the radar noise factor, k_B is the Stefan–Boltzmann constant, T_0 is the temperature, B is the radar receiver bandwidth, L_R is the internal losses of the radar, P_T is the transmit power, G is the antenna gain, G_{SP} is the signal processing gain, G_I is the integration gain, λ is the radar's wavelength, and F_b is the propagation factor. We have assumed that the radar does not use pulse compression techniques and have therefore set $G_{\mathrm{SP}} = 0$ dB.

Using Eq. (12) together with the estimated parameter values of the Mineral-U radar (Table 1) and the calculated values of the propagation factor F_b at the expected distance and height of the warship, we can estimate the smallest RCS detectable by the radar. If this value is smaller than the estimated RCS of the *Moskva*, the radar would have detected the warship.

Results

We start by examining the atmospheric conditions in the region of interest for 12–14 April 2022. Figure 3a shows the average values of the vertical gradient of the modified refractivity profiles between the radar and the warship. From Fig. 3a it can be seen that $dM/dH < 0$ at 1700 LT 13 April 2022, indicating that the atmospheric conditions at this time allowed radar waves to be trapped. Further, a diurnal cycle of dM/dH can be seen near the surface, with smaller values of dM/dH occurring in the afternoons. Figure 3b shows the surface pressure for the same time period, which ranged from 1,012 to 1,021 hPa. Figure 3c depicts the difference in partial pressure of water vapor between the lowest pressure level and the surface, together with dM/dH at sea level. The difference in partial pressure of water vapor exhibits a diurnal variation similar to dM/dH at sea level, indicating that the second term in Eq. (6) dominated the contribution to dM/dH during this time period. Figure 3d shows the difference between the temperature at the lowest pressure level and the 2-m temperature.

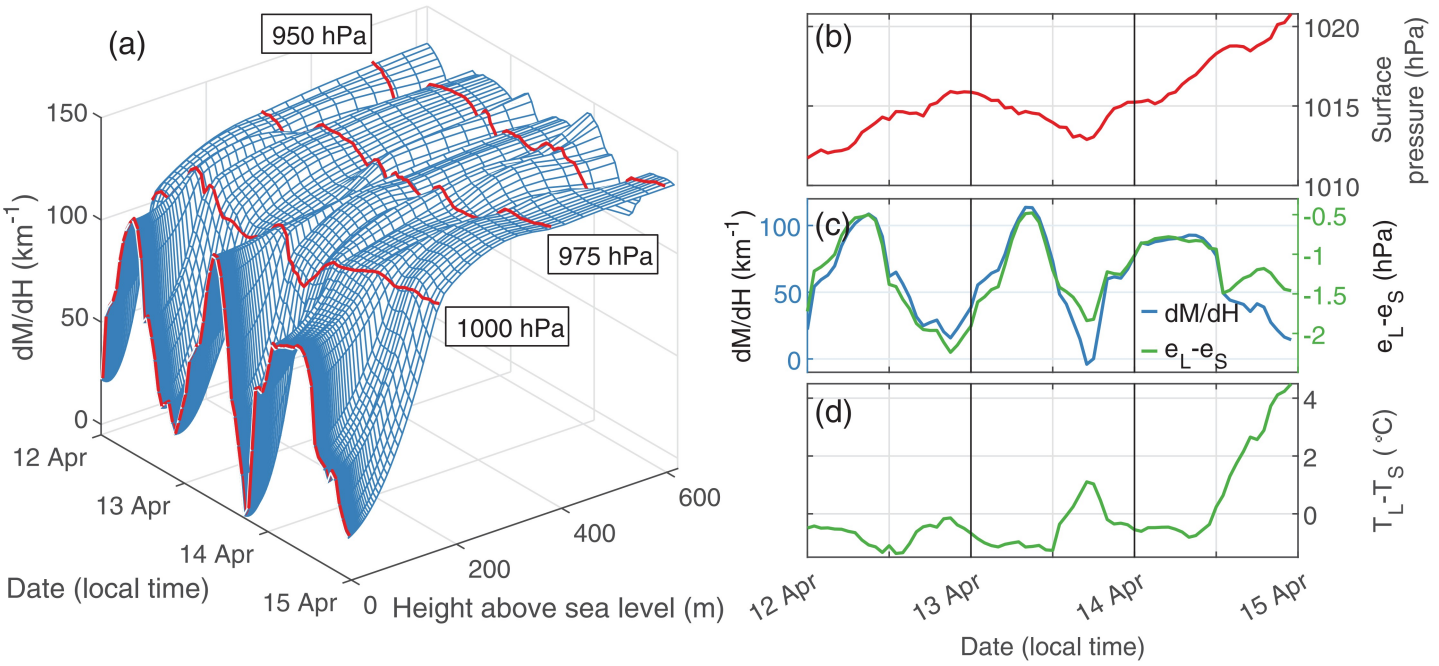

Fig. 3. Mean values of some parameters for the distance between the location of the Mineral-U radar and the warship *Moskva*. (a) Vertical gradient of the modified atmospheric refractivity for the period 12–14 Apr 2022, as a function of time and height above sea level. Red lines show the height of the surface layer and the three lowest pressure levels. (b) Surface pressure. (c) Difference between the partial pressure of water vapor at the lowest pressure level (1,000 hPa), e_L, and the partial pressure of water vapor at the surface, e_s, together with the vertical gradient of the modified atmospheric refractivity at sea level. (d) Difference between the temperature at the lowest pressure level T_L and the 2-m temperature T_S.

In the afternoons of 13 and 14 April 2022, a temperature inversion can be seen, leading to a further decrease in dM/dH.

Let us now examine the atmospheric conditions along the distance from the radar to the warship at the time of the missile launch. Figure 4 shows the pressure, temperature, partial pressure of water vapor, wind speed, wind direction, and the vertical gradient of the modified atmospheric refractivity between the Mineral-U radar and the warship *Moskva* along the path shown in Fig. 2, at 1600 LT 13 April 2022. From Fig. 4a it is seen that the pressure increased slightly with decreasing latitude. A temperature inversion can be seen (Fig. 4b), extending all the way out to the warship. The partial pressure of water vapor decreased rapidly with increasing heights for all latitudes (Fig. 4c). Wind strength, shown in Fig. 4d, increased from 8 to 9 m s^{-1} at the surface up to 12 m s^{-1} at 100 m above sea level. The wind direction was broadly to the southeast with winds turning slightly eastward for decreasing latitudes (Fig. 4e). In the lowest 100 m above sea level, atmospheric propagation conditions corresponded to superrefraction (Fig. 4f). It is clear that below 100 m above sea level the atmospheric conditions were far from normal and that a large impact on the propagation of electromagnetic waves can be expected.

Using the vertical refractivity profiles together with the assumed altitude and beamwidth of the Mineral-U radar, we can apply the electromagnetic wave propagation model to calculate the propagation factor F_b (assuming no surface roughness). Figure 5 shows F_b, based on the atmospheric conditions at 1600 LT 13 April 2022. The figure shows that F_b, at 20 m above sea level and at a distance of 135 km, is around 1 dB due to the superrefractive conditions. This means that at that time and distance, more energy was located at that height above the sea than in the radar's main lobe in free space.

Extracting the maximum value of F_b from the sea surface up to 20 m above sea level for all distances and all hours of the day on 13 April 2022, we calculated the smallest RCS detectable by the Mineral-U radar using Eq. (12). The results show that from 1600 to 2100 LT,

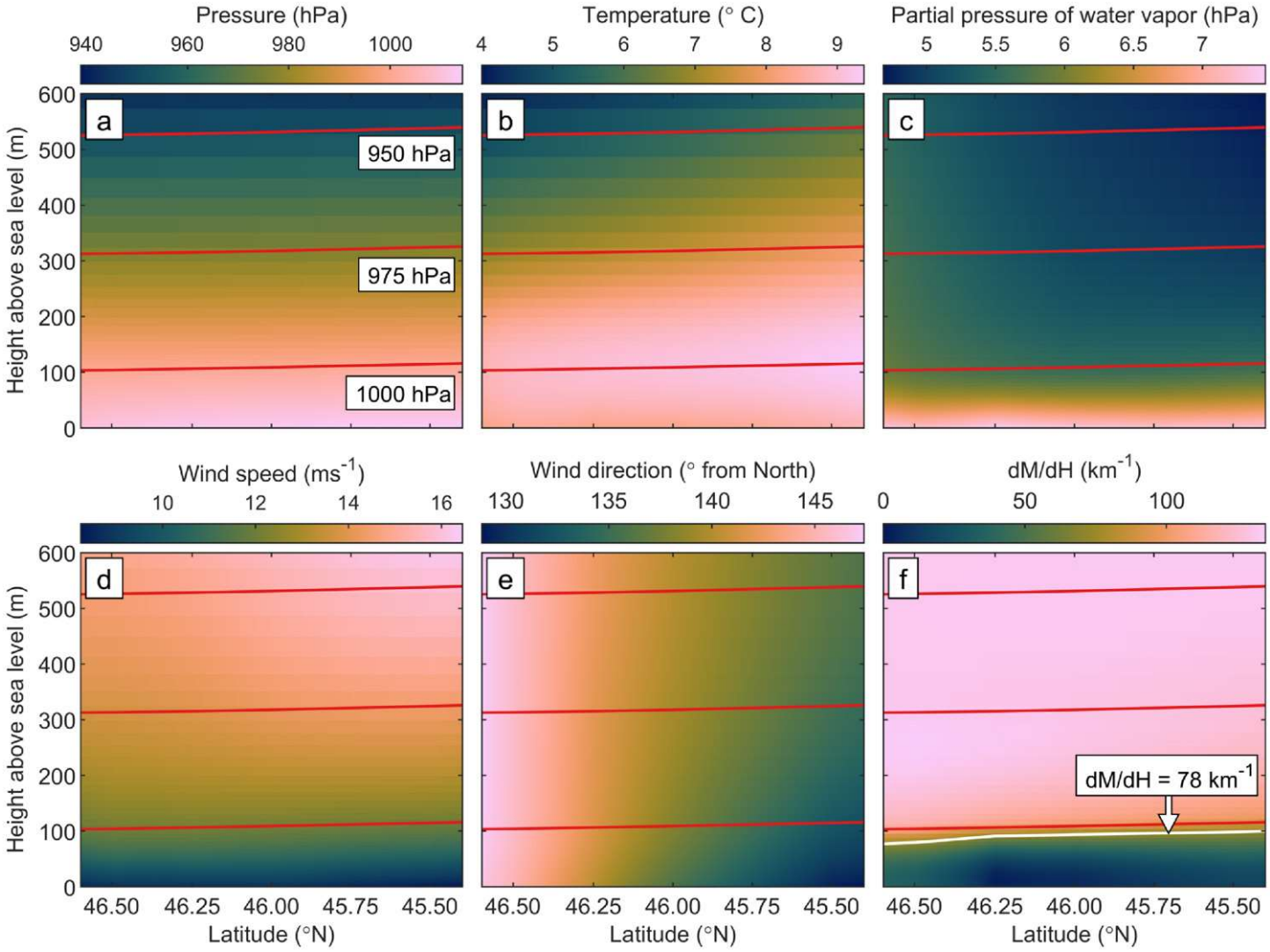

Fig. 4. Values of selected parameters for the distance between the location of the Mineral-U radar and the warship *Moskva* at 1600 LT 13 Apr 2022. (a) Atmospheric pressure. (b) Temperature. (c) Partial pressure of water vapor. (d) Wind speed. (e) Wind direction (in degrees clockwise from north). (f) Vertical gradient of the modified refractivity *dM*/*dH*. A white line indicates where superrefractive conditions end (*dM*/*dH* = 78 m s^{-1}). Red lines in all figures show the heights of the three lowest pressure levels.

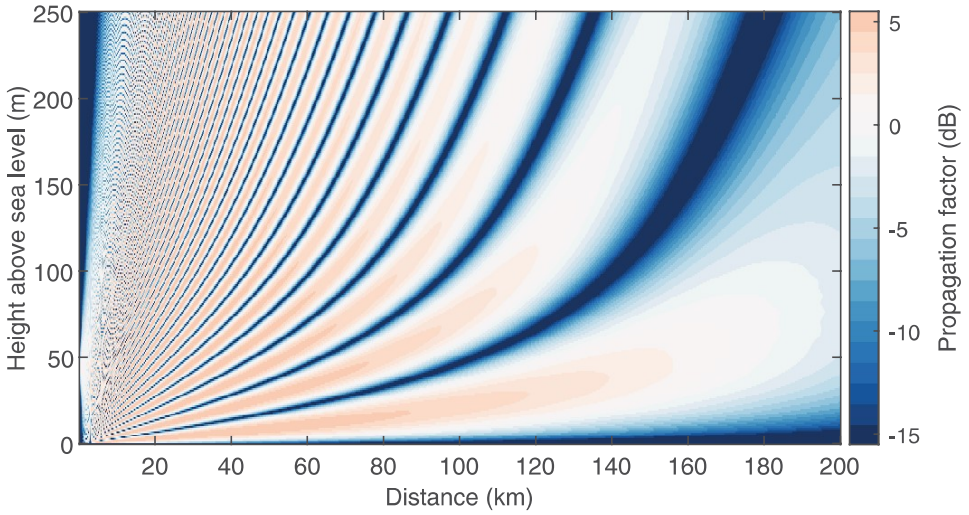

Fig. 5. Propagation factor for the Mineral-U radar (placed to the left in the figure) at 1600 LT 13 Apr 2022, using parameters from Table 1 and refractivity profiles from Fig. 3. The effect of the anomalous propagation conditions allowed energy from the radar to reach targets near the surface at a distance of well over 135 km.

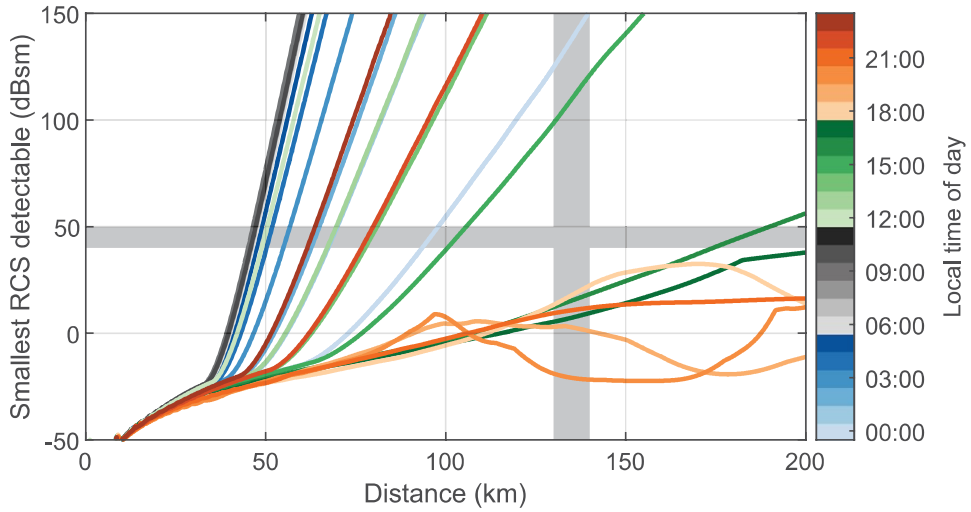

Fig. 6. Smallest RCS detectable by the Mineral-U radar for a target with a height up to 20 m above sea level on 13 Apr 2022. The different lines correspond to different hours of 13 Apr 2022. The estimated RCS of the warship *Moskva* (40–50 dBsm) and its distance from the radar (130–140 km) are indicated by shaded horizontal and vertical areas. A target with the estimated RCS of the *Moskva* could be detected from 1600 to 2100 LT 13 Apr 2022.

the Mineral-U radar would have been able to detect a target with an RCS greater than 20 dBsm for distances up to at least 135 km (Fig. 6). Since we estimate the broadside RCS of *Moskva* to be between 40 and 50 dBsm we conclude that the Mineral-U radar would easily have been able to detect the warship in the afternoon and evening on 13 April 2022, but not earlier (or later) in the day. The targeting of the warship therefore seems to have occurred as soon as the atmospheric propagation conditions allowed for detection.

Discussion

Several potential sources of uncertainties may affect the results presented in the previous section. First, the results rely on an accurate description of the atmosphere. Second, assumptions and simplifications in the electromagnetic wave propagation model can also affect the results. Third, several parameters of the Mineral-U radar are unknown as is the RCS of the warship *Moskva*. Finally, the positions of both the radar system and the warship are subject to uncertainties.

Let us first discuss the atmospheric description, here represented by the ERA5 reanalysis dataset. Inaccuracies in the ERA5 dataset could lead to changes in the vertical gradient of the atmospheric refractivity, which in turn would affect the propagation of radar waves. One way to assess the accuracy of the ERA5 dataset is to compare the data to satellite imagery. The satellite images from MSG show that the large-scale meteorological conditions for 13 April 2022 (Fig. 1) are consistent with the ERA5 datasets.

Another way to assess ERA5 is to make an intercomparison with a different reanalysis dataset. We have compared the ERA5 dataset with the Modern-Era Retrospective Analysis for Research and Applications, version 2 (MERRA-2) reanalysis dataset, provided by NASA (Gelaro et al. 2017). The intercomparison revealed that the two datasets indeed are very similar (for details, see appendix A). The results in the previous section show that on 13 April 2022, superrefractive conditions were limited to the lowermost 100 m. However, due to limited vertical resolution of the ERA5, any potential elevated duct would have been difficult to resolve.

Statistically, it is known that ducting and superrefractive conditions are more common in the spring and summer than in the winter (von Engeln and Teixeira 2004; Lopez 2009; Sirkova 2015; Magaldi et al. 2016; H. Wang et al. 2018; Norin 2023). To see

whether the propagation conditions in the Black Sea showed similar characteristics in the spring 2022, we calculated the detectability of the warship for the positions shown in Fig. 2 from 1 February to 30 April 2022, using the ERA5 dataset. The results show that in February 2022, the warship would only have been detected during a few days. From the end of March until the end of April, ducting or superrefractive conditions occurred with irregular intervals during several days, making detection possible. For details, see appendix B.

The electromagnetic wave propagation model used in this work, Detvag, uses a two-dimensional field of the atmospheric index of refraction and can also take into account terrain effects. However, we do not have a high-resolution terrain model for the northern Black Sea coast, and since the Mineral-U radar likely was located near the shoreline, we have assumed that the surface consisted of seawater for the entire distance from the radar to the warship. Sea surface roughness can influence the propagation of radar waves (Lentini and Hackett 2015; Penton and Hackett 2018). The assumption of no surface roughness is therefore a source of uncertainty in the results.

Other uncertainties originate from the unknown parameters of the Mineral-U radar system and the unknown RCS of the warship *Moskva*. Even though we have used our best estimates for all radar parameters, they may still be incorrect. Adjusting any of the radar parameters leads to changes in Eq. (12), thereby increasing or decreasing the minimum detectable RCS, σ_{min}.

The value of σ_{min} should be compared to the estimated RCS of the warship *Moskva*. The RCS of the *Moskva* changes with both aspect and pitch angles and a complete analysis of the situation would require full 3D knowledge of the warship's RCS, together with a more accurate way to calculate the reflected radar energy. However, the results in Fig. 6 show a wide margin (20–30 dB) between the assumed RCS of the *Moskva* and σ_{min}, leaving room for some errors in the radar parameter estimation.

Finally, the results in the previous section show that the Mineral-U radar would have been able to detect the warship *Moskva* at the time of the missile launch. The results rely on the validity of the atmospheric description but also on the estimated positions and heights of both the Mineral-U radar as well as of the warship *Moskva* at the time of the missile launch. To check the robustness of the results, we have analyzed four alternative positions of both the radar and the warship as well as different altitudes of the radar antenna and different heights of the warship (see appendix C).

Our analyses show the radar position did not have a significant impact on the result. Furthermore, the warship would have been detected at all examined positions, albeit at slightly different times of the day. The antenna altitude did not have a large impact on the radar's ability to detect the *Moskva*. However, for very low antenna altitudes (below 20 m) the radar would have struggled to detect the warship. The analyses also show that the higher the warship, the easier for the radar to detect. Low warship heights (below 10 m) in combination with low antenna altitudes (below 30 m) would have made detection of the warship difficult.

Conclusions

On the afternoon of 13 April 2022, explosions occurred on the Russian warship *Moskva*, and the ship subsequently sank in the Black Sea the next day. Ukraine claims to have hit the warship with two R-360 Neptune anti-ship missiles, launched from the coastline near Odesa. Since the *Moskva* at the time was located some 135 km from the coast, it has been a question of some debate how the missile's targeting radar, Mineral-U, could have been able to detect the warship, as the detection distance under standard atmospheric conditions extends to less than 50 km.

In a newspaper article published in the *Ukrainska Pravda* (Romaniuk 2022), the reason for the detection was attributed to the special weather conditions that were present at the time. In this work, we have examined this claim by calculating the atmospheric refractivity from meteorological reanalysis data and thereafter applying an electromagnetic wave propagation model. We found that at the time of the missile launch the atmospheric conditions were indeed allowing a ground-based radar to detect targets close to the sea surface at much longer distances than normal.

While we cannot determine the events that transpired on the afternoon of 13 April 2022 leading to the *Moskva* sinking, we can conclude that, given the atmospheric conditions obtained from meteorological reanalysis data, it would have been possible for a ground-based radar to detect the warship at a distance of well over 135 km.

The results show that atmospheric conditions must be considered carefully, even during warfare, as their impact on radar wave propagation can be considerable. With increasingly detailed and accurate meteorological reanalysis data available, it is now possible to perform in-depth analyses of past atmospheric propagation conditions. In this work, we have focused on a single military event, albeit one that received a great deal of attention. Military analysts and civil incident investigation boards can likely find other events that can be clarified and better understood when supported by reanalyzed meteorological data.

Acknowledgments. This work was supported by the Swedish Defence Materiel Administration (Försvarets materielverk, FMV), Grant 5002948. The scientific color maps used in the article were created by Brewer (2023) and Crameri (2021). The maps in Figs. 2 and C1 were generated using the software package M_Map (Pawlowicz 2021). The authors gratefully acknowledge insightful and constructive comments from three anonymous reviewers.

Data availability statement. ERA5 reanalysis data are available from the ECMWF Climate Data Store. The MERRA-2 reanalysis data are available from NASA Global Modeling and Assimilation Office. Satellite images from MSG/SEVIRI are available from EUMETSAT. Details about Detvag, the electromagnetic wave propagation model, have been published (Asp et al. 1997; Holm 2007) and the settings used in this work are described in the text. The code itself is not publicly available.

Appendix A: Intercomparison of meteorological data

The Modern-Era Retrospective Analysis for Research and Applications, version 2 (MERRA-2) is a reanalysis dataset, provided by NASA (Gelaro et al. 2017). In addition to forecast data, MERRA-2 assimilates other datasets, such as modern hyperspectral radiance and microwave observations, GPS radio occultation, and NASA's ozone profile observations. We have used data for pressure levels (Global Modeling and Assimilation Office 2015b) as well as surface level data (Global Modeling and Assimilation Office 2015a). The temporal resolution of the MERRA-2 pressure level dataset is 3 h, and the spatial resolution is around 50 km in the latitudinal direction.

To assess the similarity between the data from ERA5 and MERRA-2, we have made an intercomparison. Figure A1 shows vertical profiles of the temperature, specific humidity, and the vertical gradient of the modified atmospheric refractivity for the period 12–14 April 2022 for both datasets at a common grid point in the Black Sea (46.0°N, 31.25°E). Figure A1 shows that the datasets are qualitatively similar.

For a more quantitative comparison, the pairwise difference between several parameters at some common pressure levels (975, 950, 925, 900, 875, and 850 hPa) and common grid points (latitudes 45.0°, 45.5°, 46.0°, and 46.5°N, longitude 31.25°E) were calculated every third hour (the time resolution of the MERRA-2 dataset) for the period 1–30 April 2022. Table A1 shows the mean and standard deviation of the difference in temperature, partial

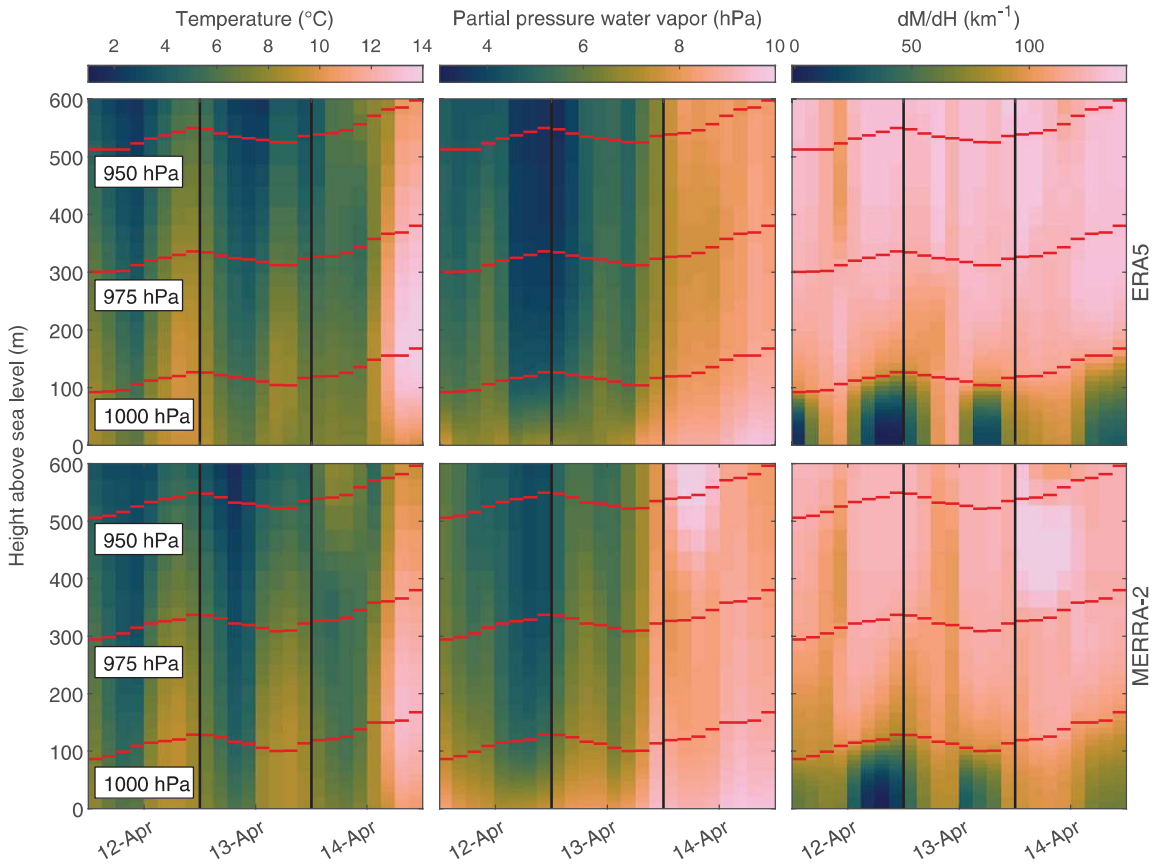

Fig. A1. Comparing reanalysis data from ERA5 with data from MERRA-2. Vertical profiles of temperature, partial pressure of water vapor, and the vertical gradient of the modified atmospheric refractivity at a common grid point (46.0°N, 31.25°E), for the period 12–14 Apr 2022. The upper row shows data from the ERA5 reanalysis dataset, the lower row shows the corresponding data from the MERRA-2 reanalysis dataset. Red lines show the heights of the three lowest pressure levels.

pressure of water vapor, pressure level heights, as well as the difference in surface pressure. The results show that the two datasets are quantitatively similar.

Appendix B: Long-term analysis of anomalous propagation conditions

To see if the ERA5 datasets provide varying wave propagation conditions during different times of the year, we calculated the smallest RCS detectable by the Mineral-U radar (the same analysis as the one performed in the "Results" section) for the period 1 February 2022–30 April 2022. The smallest RCS detectable by the Mineral-U radar as a function of distance is shown in Fig. B1.

The results show that in February 2022, ducting or superrefractive conditions only occurred during a few days. From the end of March until the end of April, ducting or superrefraction occurred with irregular intervals during several days. It is worth noting that the

Table A1. Mean and standard deviation of the pairwise difference between parameters from ERA5 and MERRA-2 at common pressure levels and common grid points near the path from the radar to the warship, for 1–30 Apr 2022. Parameters with subscript *L* originate from pressure levels whereas parameters with subscript *S* originate from surface parameters. Here, ΔT is the difference in temperature (K), Δe is the difference in partial pressure of water vapor (hPa), ΔH is the difference in pressure level heights (m), and Δp is the difference in surface pressure (hPa).

	ΔT_L	Δe_L	ΔH	ΔT_S	Δe_S	Δp
μ	−0.072	−0.31	−2.1	0.0042	−0.29	−0.20
σ	1.1	0.89	19	1.1	0.54	0.53

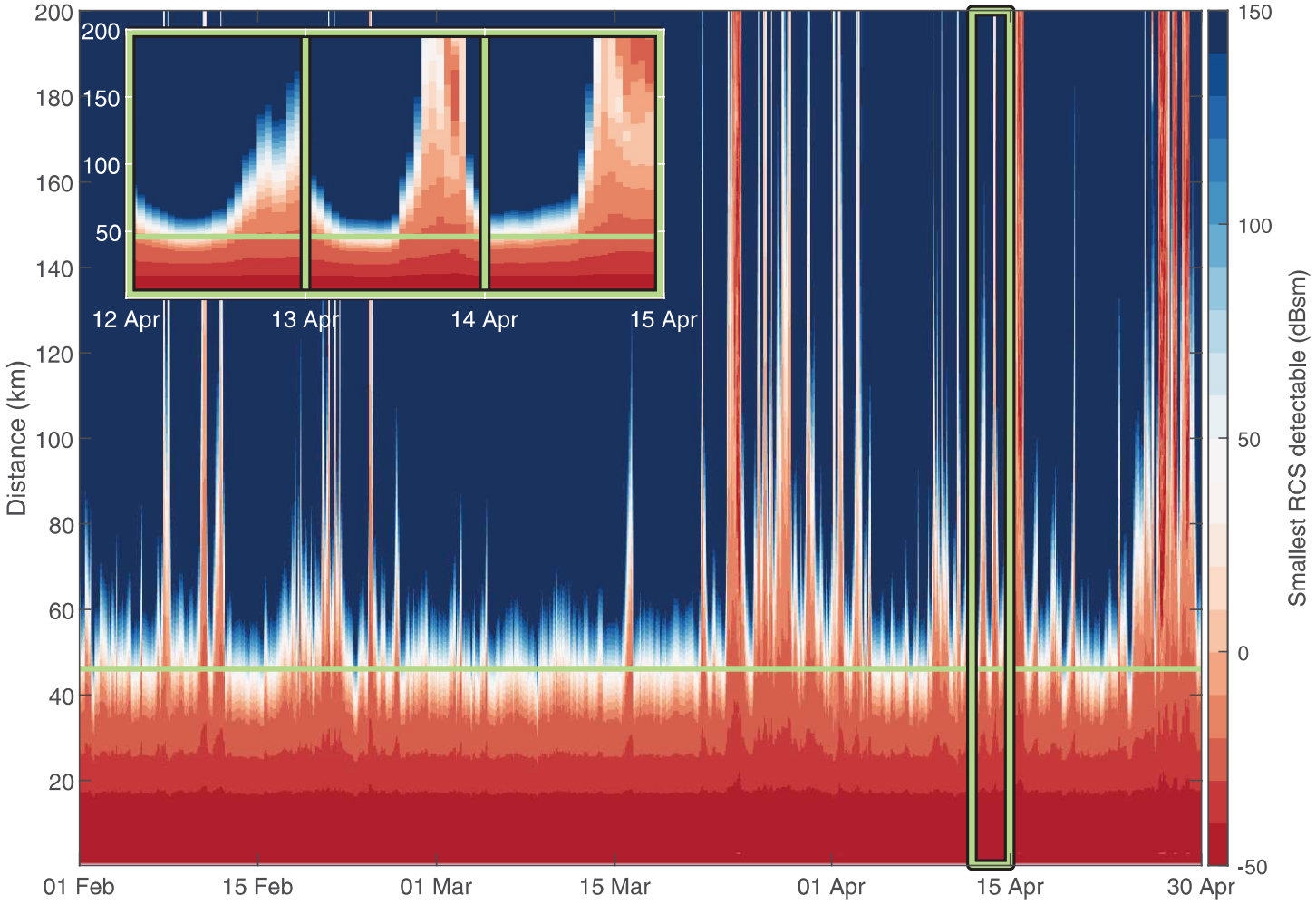

Fig. B1. Smallest RCS detectable by the Mineral-U radar for a target with a height up to 20 m above sea level as a function of distance, for the period 1 Feb 2022–30 Apr 2022. Atmospheric conditions were derived from the ERA5 reanalysis dataset. A green rectangle highlights the period 12–14 Apr 2022 (inset). A green horizontal line shows the radar horizon, found using the effective Earth radius model.

distance at which the warship would have been detected most days corresponded well to the radar horizon found using the effective Earth radius model (approximately 46 km).

Appendix C: Alternative positions and heights

Alternative positions of the radar and the warship. Since the exact locations of both the radar and the warship at the time of the missile launch are unknown, we have performed analyses using alternative positions. The calculations for radar detection were repeated for four different radar locations, ranging from near Odesa (46.575°N, 30.875°E) to the westernmost part of Mykolaiv oblast (46.625°N, 31.250°E). The warship *Moskva* was positioned at the same latitude (45.40°N) with four different longitudes, ranging from 30.50° to 31.25°E. Figure C1 shows the different positions of the radar and the warship.

Vertical profiles of atmospheric refractivity were calculated between the position of the radar and the warship for 13 April 2022, as described in the section "Vertical profiles of the atmospheric index of refraction." The minimum detectable RCS for target heights up to 20 m above sea level as a function of the time of day, for all positions of the radar and the warship, is shown in Fig. C2. The results show the radar position did not have a significant impact on the result. Furthermore, the warship would have been detected at all examined positions, but at slightly different times of the day.

If the warship would have been located at the westernmost position (position 1), the radar would have detected it already at 1500 LT. If the warship was in position 2 (used for the analysis in the "Results" section) or position 3, it would have been detected at 1600 LT, whereas if it had been in position 4 it would not have been detected until 1800 LT in the evening. After 2100 LT, the anomalous propagation conditions disappeared for all examined positions. From the results, we conclude that detection by the radar would have been possible from all examined positions, but positions 2 or 3 for the warship are most consistent with the reported time of the missile launch.

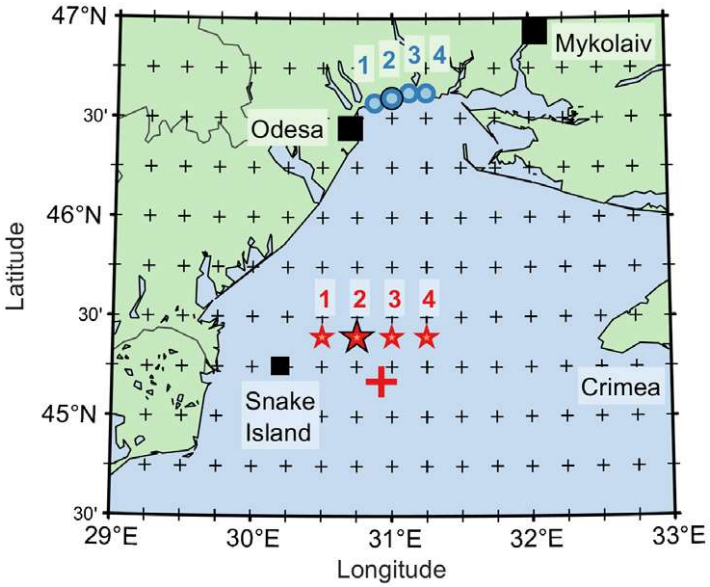

Fig. C1. Map over the Black Sea showing alternative positions for the Mineral-U radar (blue circles) and the warship *Moskva* (red stars) at the time of the anti-ship missile launch. Position number 2 was used both for the radar and for the warship in the "Results" section (corresponding markers are outlined in black). The large red plus sign marks where the *Moskva* was located by satellite at 1852 LT 13 Apr 2022. Small black plus signs show grid points of the ERA5 reanalysis dataset.

Alternative antenna altitudes and warship heights. The altitude of the radar antenna at the time of the missile launch is unknown. To investigate the impact of alternative antenna altitudes we performed calculations in which the antenna altitude was varied from 15 to 80 m above sea level. The results show that the antenna altitude did not have a large impact on the radar's ability to detect the warship. However, for very low antenna altitudes (below 20 m) the radar would have struggled to detect the warship.

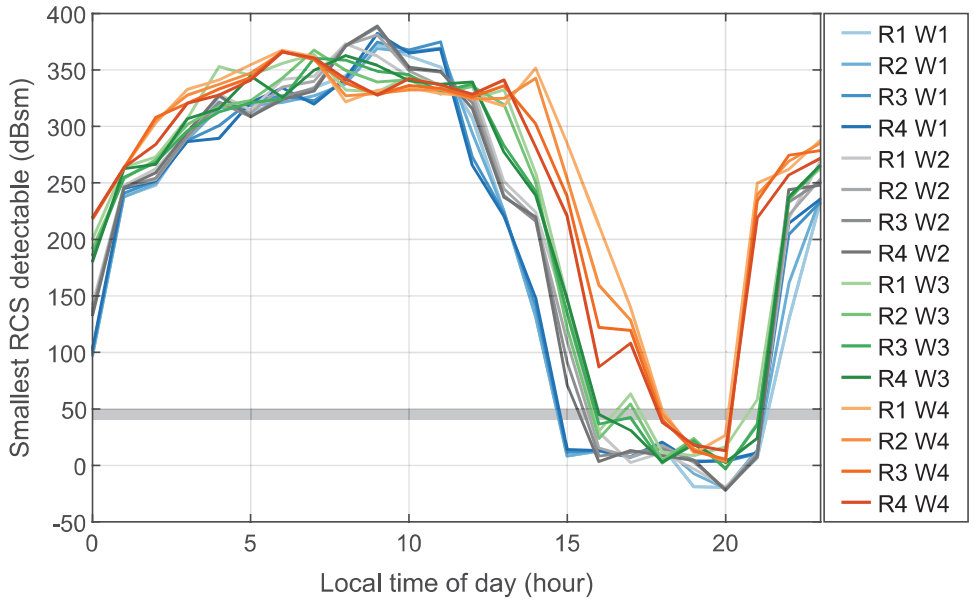

Fig. C2. Smallest RCS detectable by the Mineral-U radar for alternative positions, on 13 Apr 2022. RCS are evaluated up to 20 m above sea level and at 135 km distance from the radar. The different positions of the radar (R) and the warship (W) are shown in the legend (see map in Fig. C1). Radar parameters are given by Table 1. The estimated RCS of the warship *Moskva* (40–50 dBsm) is indicated by a shaded horizontal area.

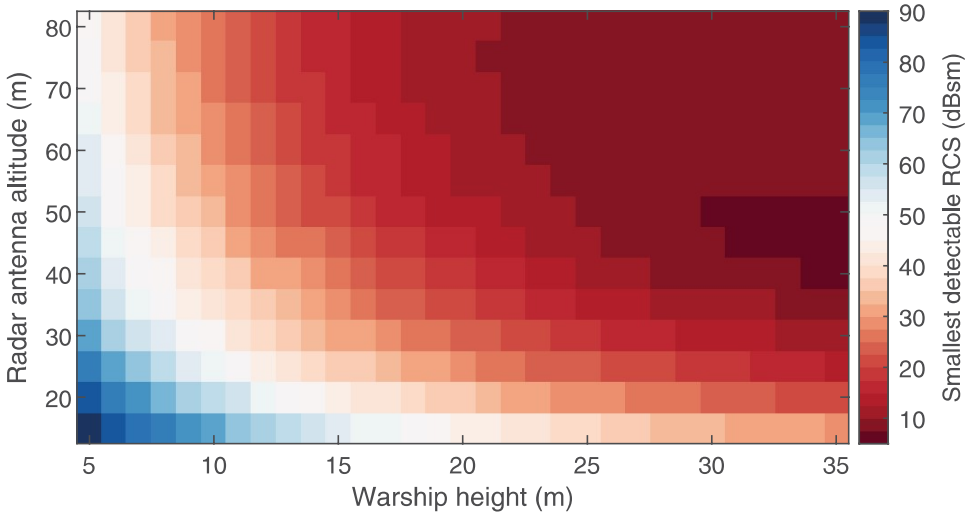

Fig. C3. Smallest RCS detectable by the Mineral-U radar for different antenna altitudes and warship heights. RCS are evaluated at 135 km distance from the radar at 1600 LT 13 Apr 2022. Results are shown for different altitudes of the radar antenna as well as for different heights above sea level of the warship. Radar parameters are given by Table 1. The estimated RCS of the warship *Moskva* is 40–50 dBsm.

Another factor that influences the analysis is the height above sea level up to which the propagation factor should be examined. As the RCS of the warship varies with both aspect and pitch angles, a complete analysis of the event would require full 3D knowledge of the warship's RCS. Here we have instead used the maximum value of the propagation factor up to a certain height above the sea surface. In the "Results" section, we used the maximum value of the propagation factor up to 20 m above sea level.

To investigate how the results change when using a different maximum height of the warship the same analysis was performed, where the maximum height was varied from 5 to 35 m. The analysis shows that the higher the warship, the easier for the radar to detect. Low warship heights (below 10 m) in combination with low radar antenna altitudes (below 30 m) would have made detection of the warship difficult.

The results of both the alternative antenna altitudes and the alternative warship heights are shown in Fig. C3.

References

Anderson, K., and Coauthors, 2004: The RED experiment: An assessment of boundary layer effects in a trade winds regime on microwave and infrared propagation over the sea. *Bull. Amer. Meteor. Soc.*, **85**, 1355–1366, https://doi.org/10.1175/BAMS-85-9-1355.

Asp, B., G. Eriksson, and P. Holm, 1997: Detvag-90 – Final report. Defence Research Establishment Tech. Rep. FOA-R-97-00566-504-SE, 28 pp.

Battan, L. J., 1973: *Radar Observation of the Atmosphere.* The University of Chicago Press, 324 pp.

Bean, B. R., and E. J. Dutton, 1966: *Radio Meteorology.* U.S. Government Printing Office, 435 pp.

Brewer, C. A., 2023: ColorBrewer 2.0: Color advice for cartography. Accessed 15 May 2023, https://colorbrewer2.org.

Byers, H. R., 1974: *General Meteorology.* 4th ed. McGraw-Hill, 416 pp.

Cooper, H., E. Schmitt, and J. E. Barnes, 2022: U.S. Intelligence helped Ukraine strike Russian flagship, officials say. *New York Times*, 5 May, https://www.nytimes.com/2022/05/05/us/politics/moskva-russia-ship-ukraine-us.html.

Copernicus Climate Change Service, 2023a: ERA5: Compute pressure and geopotential on model levels, geopotential height and geometric height. Copernicus Climate Change Service (C3S) Climate Data Store (CDS), accessed 21 March 2023, https://confluence.ecmwf.int/display/CKB/ERA5%3A+compute+pressure+and+geopotential+on+model+levels%2C+geopotential+height+and+geometric+height.

——, 2023b: ERA5: Data documentation. Copernicus Climate Change Service (C3S) Climate Data Store (CDS), accessed 31 August 2023, https://confluence.ecmwf.int/display/CKB/ERA5\%3A+data+documentation.

——, 2023c: ERA5 hourly data on pressure levels from 1940 to present. Copernicus Climate Change Service (C3S) Climate Data Store (CDS), accessed 16 January 2023, https://doi.org/10.24381/cds.bd0915c6.

——, 2023d: ERA5 hourly data on single levels from 1940 to present. Copernicus Climate Change Service (C3S) Climate Data Store (CDS), accessed 16 January 2023, https://doi.org/10.24381/cds.adbb2d47.

Crameri, F., 2021: Scientific colour maps, version 7.0.1. Zenodo, accessed 15 May 2023, https://doi.org/10.5281/zenodo.5501399.

Defense Express, 2021a: Initial two BLOS radars for Neptune ASCM system to be delivered by year's end. Defense Express, accessed 1 June 2023, https://en.defence-ua.com/news/initial_two_blos_radars_for_neptune_ascm_system_to_be_delivered_by_years_end-1903.html.

——, 2021b: Mineral-U, a support radar for Neptune ASCM's, succeeds through industry trials. Defense Express, accessed 1 June 2023, https://en.defence-ua.com/news/mineral_u_a_support_radar_for_neptune_ascms_succeeds_through_industry_trials-1997.html.

Dockery, D., and J. R. Kuttler, 1996: An improved impedance-boundary algorithm for Fourier split-step solutions of the parabolic wave equation. *IEEE Trans. Antennas Propag.*, **44**, 1592–1599, https://doi.org/10.1109/8.546245.

Dockery, G. D., 1988: Modeling electromagnetic wave propagation in the troposphere using the parabolic equation. *IEEE Trans. Antennas Propag.*, **36**, 1464–1470, https://doi.org/10.1109/8.8634.

Doviak, R. J., and D. D. Zrnić, 2006: *Doppler Radar and Weather Observations.* 2nd ed. Dover Publications, 562 pp.

EUMETSAT, 2023: SEVIRI airmass RGB quick guide. European Organisation for the Exploitation of Meteorological Satellites, accessed 17 August 2023, https://www.eumetsat.int/media/41623.

EUMETView, 2023: EUMETSAT data services. European Organisation for the Exploitation of Meteorological Satellites, accessed 21 March 2023, https://view.eumetsat.int.

Forgey, Q., and M. Ward, 2022: Pentagon confirms explosion aboard Russian warship. POLITICO, accessed 1 June 2023, https://www.politico.com/news/2022/04/14/pentagon-explosion-russian-warship-00025243.

Gelaro, R., and Coauthors, 2017: The Modern-Era Retrospective Analysis for Research and Applications, version 2 (MERRA-2). *J. Climate*, **30**, 5419–5454, https://doi.org/10.1175/JCLI-D-16-0758.1.

Genova, J., 2018: *Electronic Warfare Signal Processing.* 1st ed. Artech House, 612 pp.

Gesch, D. B., K. L. Verdin, and S. K. Greenlee, 1999: New land surface digital elevation model covers the Earth. *Eos, Trans. Amer. Geophys. Union*, **80**, 69–70, https://doi.org/10.1029/99EO00050.

Global Modeling and Assimilation Office, 2015a: MERRA-2 inst1_2d_asm_nx: 2d, 1-hourly, instantaneous, single-level, assimilation, single-level diagnostics v5.12.4. Goddard Earth Sciences Data and Information Services Center (GES DISC), accessed 16 February 2023, https://doi.org/10.5067/3Z173KIE2TPD.

——, 2015b: MERRA-2 inst3_3d_asm_np: 3d, 3-hourly, instantaneous, pressure-level, assimilation, assimilated meteorological fields v5.12.4. Goddard Earth Sciences Data and Information Services Center (GES DISC), accessed 16 February 2023, https://doi.org/10.5067/QBZ6MG944HW0.

Grey zone, 2022: Telegram post. Telegram, accessed 1 June 2023, https://t.me/grey_zone/13646.

Haack, T., C. Wang, S. Garrett, A. Glazer, J. Mailhot, and R. Marshall, 2010: Mesoscale modeling of boundary layer refractivity and atmospheric ducting. *J. Appl. Meteor. Climatol.*, **49**, 2437–2457, https://doi.org/10.1175/2010JAMC2415.1.

Hallam, J., B. Lendon, U. Pavlova, and I. Kottasová, 2022: New photos show Russian warship Moskva before it sank. CNN, accessed 1 June 2023, https://edition.cnn.com/2022/04/18/europe/ukraine-moskva-warship-sinking-images-intl/index.html.

Hannen, P. J., 2014: *Radar and Electronic Warfare Principles for the Non-Specialist.* SciTech Publishing, 388 pp.

Harding, L., P. Beaumont, P. Sauer, J. Elgot, and J. Borger, 2022: Russian warship Moskva on fire but afloat, Pentagon says. *Guardian*, 14 April, https://www.theguardian.com/world/2022/apr/14/russia-moskva-ship-ukraine-black-sea.

Hersbach, H., and Coauthors, 2018a: ERA5 hourly data on pressure levels from 1940 to present. Copernicus Climate Change Service (C3S) Climate Data Store (CDS), accessed 16 January 2023, https://doi.org/10.24381/cds.bd0915c6.

——, and Coauthors, 2018b: ERA5 hourly data on single levels from 1940 to present. Copernicus Climate Change Service (C3S) Climate Data Store (CDS), accessed 16 January 2023, https://doi.org/10.24381/cds.adbb2d47.

Holm, P. D., 2007: Wide-angle shift-map PE for a piecewise linear terrain – A finite-difference approach. *IEEE Trans. Antennas Propag.*, **55**, 2773–2789, https://doi.org/10.1109/TAP.2007.905865.

Kerr, D., 1951: *Propagation of Short Radio Waves.* McGraw-Hill, 728 pp.

Knott, E. F., J. F. Shaeffer, and M. T. Turley, 2004: *Radar Cross Section.* 2nd ed. SciTech Publishing, 612 pp.

Kulessa, A. S., and Coauthors, 2017: The Tropical Air–Sea Propagation Study (TAPS). *Bull. Amer. Meteor. Soc.*, **98**, 517–537, https://doi.org/10.1175/BAMS-D-14-00284.1.

Kuttler, J. R., and G. D. Dockery, 1991: Theoretical description of the parabolic approximation/Fourier split-step method of representing electromagnetic propagation in the troposphere. *Radio Sci.*, **26**, 381–393, https://doi.org/10.1029/91RS00109.

Lawrence, M. G., 2005: The relationship between relative humidity and the dewpoint temperature in moist air: A simple conversion and applications. *Bull. Amer. Meteor. Soc.*, **86**, 225–234, https://doi.org/10.1175/BAMS-86-2-225.

Lentini, N. E., and E. E. Hackett, 2015: Global sensitivity of parabolic equation radar wave propagation simulation to sea state and atmospheric refractivity structure. *Radio Sci.*, **50**, 1027–1049, https://doi.org/10.1002/2015RS005742.

Levy, M. F., 2000: *Parabolic Equation Methods for Electromagnetic Wave Propagation.* Institution of Electrical Engineers, 352 pp.

Lopez, P., 2009: A 5-yr 40-km-resolution global climatology of superrefraction for ground-based weather radars. *J. Appl. Meteor. Climatol.*, **48**, 89–110, https://doi.org/10.1175/2008JAMC1961.1.

Magaldi, A., M. Mateu, J. Bech, and J. Lorente, 2016: A long term (1999–2008) study of radar anomalous propagation conditions in the western Mediterranean. *Atmos. Res.*, **169**, 73–85, https://doi.org/10.1016/j.atmosres.2015.09.027.

MathWorks, 2023: MATLAB function reference R2023b. The MathWorks Inc., 18 646 pp., https://se.mathworks.com/help/pdf_doc/matlab/matlab_ref.pdf.

McGillvray, J. W., 1994: Stealth technology in surface warships. *Nav. War Coll. Rev.*, **47**, 28–39.

Norin, L., 2023: Observations of anomalous propagation over waters near Sweden. *Atmos. Meas. Tech.*, **16**, 1789–1801, https://doi.org/10.5194/amt-16-1789-2023.

Pastore, D. M., D. P. Greenway, M. J. Stanek, S. E. Wessinger, T. Haack, Q. Wang, and E. E. Hackett, 2021: Comparison of atmospheric refractivity estimation methods and their influence on radar propagation predictions. *Radio Sci.*, **56**, e2020RS007244, https://doi.org/10.1029/2020RS007244.

Patterson, W. L., 2008: The propagation factor, F_p, in the radar equation. *Radar Handbook*, 3rd ed. M. Skolnik, Ed., McGraw-Hill, 26.1–26.28.

Pawlowicz, R., 2021: M_map: A mapping package for Matlab, version 1.4n. Accessed 15 May 2023, http://www.eoas.ubc.ca/~rich/map.html.

Penton, S. E., and E. E. Hackett, 2018: Rough ocean surface effects on evaporative duct atmospheric refractivity inversions using genetic algorithms. *Radio Sci.*, **53**, 804–819, https://doi.org/10.1029/2017RS006440.

Romaniuk, R., 2022: Sinking the Moskva: Previously undisclosed details. How the Ukrainian Neptune destroyed the flagship of the Russian fleet. *Ukrainska Pravda*, 13 December, https://www.pravda.com.ua/eng/articles/2022/12/13/7380452.

Sirkova, I., 2015: Duct occurrence and characteristics for Bulgarian Black sea shore derived from ECMWF data. *J. Atmos. Sol.-Terr. Phys.*, **135**, 107–117, https://doi.org/10.1016/j.jastp.2015.10.017.

Skolnik, M. I., 2001: *An Introduction to Radar Systems.* 3rd ed. McGraw-Hill, 772 pp.

Smith, E. K., and S. Weintraub, 1953: The constants in the equation for atmospheric refractive index at radio frequencies. *J. Res. Natl. Bur. Stand.*, **50**, 39–41, https://doi.org/10.6028/jres.050.006.

Sutton, H. I., 2022: Satellite image pinpoints Russian cruiser Moskva as she burned. *Naval News*, 15 April, https://www.navalnews.com/naval-news/2022/04/satellite-image-pinpoints-russian-cruiser-moskva-as-she-burned.

Turton, J. D., D. A. Bennetts, and S. F. G. Farmer, 1988: An introduction to radio ducting. *Meteor. Mag.*, **117**, 245–254.

Tyler, R., T. Boyer, T. Minami, M. M. Zweng, and J. R. Reagan, 2017: Electrical conductivity of the global ocean. *Earth Planets Space*, **69**, 156, https://doi.org/10.1186/s40623-017-0739-7.

Ukrainian Defence Industry, 2020a: Electronic warfare, surveillance and target detection systems. 28 pp., https://ukrspecexport.com/uploads/files/Categories/pdf_3/92176e.pdf.

——, 2020b: Radar, radio communication and defence systems. 44 pp., http://progress.gov.ua/wp-content/uploads/2020/08/radar-radio-communication-and-air-defence-systems.pdf.

Ukrinform, 2022: Russian cruiser Moskva capsized and began to sink – Operational Command South. Ukrinform, accessed 1 June 2023, https://www.ukrinform.net/rubric-ato/3457420-russian-cruiser-moskva-capsized-and-began-to-sink-operational-command-south.html.

Ulate, M., Q. Wang, T. Haack, T. Holt, and D. P. Alappattu, 2019: Mean offshore refractive conditions during the CASPER east field campaign. *J. Appl. Meteor. Climatol.*, **58**, 853–874, https://doi.org/10.1175/JAMC-D-18-0029.1.

Volkmann, E., and G. Grylls, 2022: Ukraine war: US spy plane on patrol in Black Sea before sinking of Russian flagship Moskva. *Times*, 20 April, https://www.thetimes.co.uk/article/ukraine-war-us-spy-plane-on-patrol-in-black-sea-before-sinking-of-russian-flagship-moskva-fblbg0znd.

von Engeln, A., and J. Teixeira, 2004: A ducting climatology derived from the European Centre for Medium-Range Weather Forecasts global analysis fields. *J. Geophys. Res.*, **109**, D18104, https://doi.org/10.1029/2003JD004380.

Wang, H., G. Wang, and L. Liu, 2018: Climatological beam propagation conditions for China's weather radar network. *J. Appl. Meteor. Climatol.*, **57**, 3–14, https://doi.org/10.1175/JAMC-D-17-0097.1.

Wang, Q., and Coauthors, 2018: CASPER: Coupled Air–Sea Processes and Electromagnetic Ducting Research. *Bull. Amer. Meteor. Soc.*, **99**, 1449–1471, https://doi.org/10.1175/BAMS-D-16-0046.1.